LIMNOLOGY and OCEANOGRAPHY

ASLO

Limnol. Oceanogr. 65, 2020, 790–806

doi: 10.1002/lno.11348

Euphotic zone nitrification in the California Current Ecosystem

Brandon M. Stephens,[1*,a] **Scott D. Wankel**,[2] **J. Michael Beman**,[3] **Ariel J. Rabines**,[4,5] **Andrew E. Allen**,[4] **Lihini I. Aluwihare**[1]

[1]Geosciences Research Division, Scripps Institution of Oceanography, University of California at San Diego, La Jolla, California
[2]Department of Marine Chemistry and Geochemistry, Woods Hole Oceanographic Institution, Woods Hole, Massachusetts
[3]Life and Environmental Sciences and Sierra Nevada Research Institute, University of California, Merced, Merced, California
[4]Microbial and Environmental Genomics Department, J. Craig Venter Institute, La Jolla, California
[5]Integrative Oceanography Division, Scripps Institution of Oceanography, University of California, San Diego, La Jolla, California

Abstract

Nitrification, the microbial conversion of ammonium to nitrite then to nitrate, occurs throughout the oceanic water column, yet the environmental factors influencing the production of nitrate in the euphotic zone (EZ) remain unclear. In this study, the natural abundances of N and O isotopes ($\delta^{15}N$ and $\delta^{18}O$, respectively) in nitrate were used in an existing model framework to quantify nitrate contributed by EZ nitrification in the California Current Ecosystem (CCE) during two anomalously warm years. Model data estimated that between 6% and 36% of the EZ nitrate reservoirs were derived from the combined steps of nitrification within the EZ. The CCE data set found nitrification contributions to EZ nitrate to be positively correlated with nitrite concentrations ($[NO_2^-]$) at the depth of the primary nitrite maximum (PNM). Building on this correlation, EZ nitrification in the southern California Current was estimated to contribute on average 20% ± 6% to EZ nitrate as inferred using the PNM $[NO_2^-]$ of the long-term California Cooperative Oceanic Fisheries Investigation (CalCOFI) survey record. A multiple linear regression analysis of the CalCOFI PNM NO_2^- time series identified two conditions that led to positive deviations in $[NO_2^-]$. Enhanced PNM $[NO_2^-]$, and potentially enhanced EZ nitrification, may be linked to (1) reduced phytoplankton competition for ammonium (NH_4^+) and NO_2^- as interpreted from particulate organic carbon:chlorophyll ratios, and/or (2) to increased supply of NH_4^+ (and then NH_4^+ oxidation to NO_2^-) from the degradation of organic nitrogen as interpreted from particulate organic nitrogen concentrations.

Throughout the Earth's biosphere microorganisms convert ammonium, the product of organic matter catabolism, into nitrite and then nitrate (Ward 2008). This process, referred to as nitrification, directly links the inputs and outputs of the global nitrogen cycle by providing the substrate necessary for the removal of N from the biosphere through anaerobic processes. During both nitrification and denitrification (conversion of nitrate to N_2), nitrous oxide (N_2O), a greenhouse gas 300 times more potent than CO_2 (Willis et al. 2007), is produced (Nevison et al. 2004). As such, environmental processes that control nitrification—especially near the ocean-atmosphere interface—are of particular interest if we are to understand the role of the marine N cycle in Earth's radiation budget.

In strong upwelling regions, nitrate enters the euphotic zone (EZ) primarily as a "new" nutrient (e.g., Chavez et al. 1989; Messié et al. 2009) and this flux is expected to be balanced by export production. The upwelling nitrate was produced by nitrification in the dark ocean and therefore represents an external source of nitrogen to the EZ (Dugdale and Goering 1967; Eppley and Peterson 1979; Messié and Chavez 2015); however, numerous observations indicate that nitrification in the EZ can also introduce nitrate to the surface ocean (Ward 1987; Ward et al. 1989; Dore and Karl 1996). Therefore, methods that rely on EZ nitrate concentrations to estimate new production (e.g., Harrison et al. 1987), and by extension the magnitude of export production, will produce erroneous results if in situ nitrification influences the nitrate reservoir in the EZ (Yool et al. 2007). Global models estimate that an average of 17% and perhaps > 30% of the surface nitrate reservoir can be derived from in situ nitrification (Yool et al. 2007; Zakem et al. 2018), though the higher estimates

*Correspondence: bmstephe@ucsd.edu and bran.step@gmail.com

Additional Supporting Information may be found in the online version of this article.

[a]Present address: Marine Science Institute, Department of Ecology, Evolution, and Marine Biology, University of California, Santa Barbara, California

Data Availability Statement: Data used in this manuscript can be found on the CCE LTER Datazoo website (http://cce.lternet.edu/data) and on the CalCOFI website (calcofi.org).

have been called into question as they rely on a handful of local studies that are unlikely to be representative of global mean nitrification rates (Peng et al. 2018). However, it is possible that these higher end estimates are more common under certain environmental conditions.

Aerobic nitrification in the open ocean typically proceeds as a two-step process. Ammonia-oxidizing *Thaumarchaeota* (referred to here as ammonia-oxidizing *Archaea* [AOA]) and to a lesser extent, ammonia-oxidizing bacteria (Ward and Carlucci 1985; Könneke et al. 2005; Schleper et al. 2005; Francis et al. 2007; Mincer et al. 2007; Santoro et al. 2010, 2018) oxidize ammonia to nitrite. Nitrite can be further oxidized to nitrate by nitrite oxidizing bacteria (NOB, e.g., Watson and Waterbury 1971; Ward and Carlucci 1985; Lücker et al. 2013). Recent studies have also isolated bacteria within the common marine genus *Nitrospira* that are capable of oxidizing both ammonia and nitrite to ultimately produce nitrate, but these organisms have not yet been detected in oligotrophic marine environments (Daims et al. 2015, 2016; Xia et al. 2018).

Ammonia and nitrite oxidation rates tend to peak (up to 60–100 nmol N L^{-1} d^{-1}) just below the 1% photosynthetically available radiation (PAR) and/or at primary nitrite maximum (PNM) depths (Ward et al. 1989; Ward 2005, 2008; Beman et al. 2008, 2012, 2013; Santoro et al. 2010), though concurrent rate estimates of ammonia and nitrite oxidation demonstrate that these two steps may at times be decoupled (Ward 1987; Beman et al. 2013). The apparent restriction of ammonia and nitrite oxidation rates and the genes associated with these conversions to low light/PNM depths has been attributed in some cases to competition with phytoplankton for ammonium and nitrite (Smith et al. 2014*b*; Zakem et al. 2018), though previous studies have also invoked the light inhibition of nitrite oxidizers (Lomas and Lipschultz 2006).

In addition to genetic- and rate-based measurements, the importance of nitrification can be determined by measuring the N and O isotope signature of nitrate ($\delta^{15}N$ and $\delta^{18}O$, respectively). The approach is based on empirical observations of processes that influence the isotopes of nitrate in surface waters. For example, during both steps of nitrification, oxygen atoms are incorporated from water into the nitrate reservoir, which results in a departure from the characteristic 1:1 slope between $\delta^{15}N$ and $\delta^{18}O$ of nitrate associated with nitrate uptake (Wankel et al. 2007; Granger and Wankel 2016). The contribution of the combined steps of nitrification to nitrate can thus be detected and quantified based on this isotopic departure. Such a method is attractive because it provides a temporally integrated estimate of nitrification not offered by rate measurements made in bottle incubations. However, quantifying nitrification from stable isotope measurements requires a model. The extent of EZ nitrification in the central California Current Ecosystem (CCE) estimated using such an isotope modeling approach (Wankel et al. 2007) was in agreement with studies that quantified nitrification rates in the same region (e.g., Ward et al. 1989; Ward 2005; Santoro et al. 2010; Smith et al. 2016).

The current study expands upon the nitrate isotope-based model of nitrification presented in Wankel et al. (2007) to better constrain the importance of EZ nitrification in the CCE. Results suggest that EZ nitrification contributed between 6% and 36% of EZ nitrate. No predictable relationship was observed with ammonium concentrations, but the fraction of nitrate derived from nitrification was positively correlated with nitrite concentrations at the PNM. This offered an opportunity to approximate past variations in nitrification using long-term nitrite records from the CalCOFI time series. Anomalous nitrite concentrations, and thus derived nitrification rates, were further examined in the context of variations in particulate organic nitrogen (PON) concentrations and phytoplankton abundance.

Materials and methods

Study location

The present study was located in the eastern North Pacific Ocean within the southern portion of the California Current System (CCS). Sample locations extended from within 20 km of Point Conception, a site of persistent upwelling, to as far as 350 km from shore (Fig. 1). Samples for this study were collected during CCE process cruises P1408 and P1604, which took place during 08 August 2014–09 September 2014 and 22 April 2016–10 May 2016, respectively. Samples were collected daily from noontime casts via Niskin bottles during coordinated experimental activities termed "Cycles." The term Cycle is used here in place of station to represent repeated, daily sampling of the same water mass rather than the sampling of a fixed location relative to the seafloor. Each Cycle

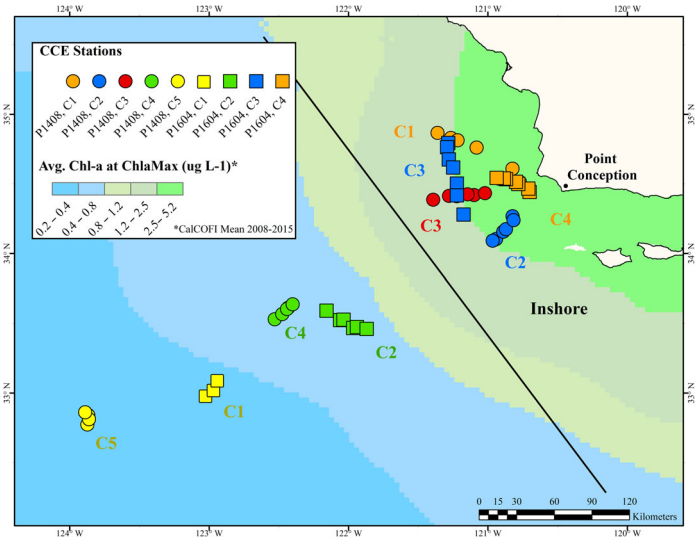

Fig. 1. Map of individual Cycles (C1, C2, etc.) for P1408 (circles) and P1604 (squares) cruises. Background blue-green colors coarsely delineate regions by Chl *a* concentrations based on the long-term interpolated CalCOFI mean Chl *a* over 2008–2015 at the Chl *a* maximum depth. Cycle colors are conserved throughout the document. The diagonal line separates "Inshore" Cycles from "Midshore" and "Offshore" Cycles.

lasted between 2 and 4 d, and a drifter array with a subsurface drogue centered around 15 m enabled the ship to nominally follow the same surface-water mass throughout the Cycle. Depth profiles extended from the surface to the 0.01% light level, typically < 150–200 m, and at least one sample was collected from > 200 m for each Cycle.

Nutrient and chlorophyll *a* concentrations

Samples for dissolved inorganic nutrient concentration measurements (expressed without brackets as NO_3^-, NO_2, and NH_4^+, to enhance readability) and chlorophyll *a* (Chl *a*) were collected on upcasts from conductivity temperature depth (CTD) Niskin bottles triggered at 10 discrete depths. These depths purposely spanned different light levels and Chl *a* distributions as estimated from CTD fluorometer profiles. Samples collected for nutrients were filtered through GF/F filters (47 mm, Whatman), frozen, and analyzed by flow injection analysis at UC Santa Barbara (https://msi.ucsb.edu/services/analytical-lab). The precision associated with nutrient concentration analysis was ± 5% and detection limits were 0.1 μmol L^{-1} for NO_2^- and NH_4^+ and 0.2 μmol L^{-1} for NO_3^-. Chl *a* was determined from GF/F filters (25 mm, Whatman) extracted with 90% acetone, and measured onboard using a Turner Designs 10 AU Fluorometer after storage for 24 h at −18°C (Goericke 2002).

$\delta^{15}N$ and $\delta^{18}O$ of nitrate

Nitrate $\delta^{15}N_{NO3}$ and $\delta^{18}O_{NO3}$ were measured on 0.7 μm-filtered (precombusted GF/F, 47 mm, Whatman) seawater collected directly from Niskin bottles and stored in 60 mL high-density polyethylene (HDPE) bottles at −80°C until analysis. Samples were analyzed on an IsoPrime 100 isotope ratio mass spectrometer with custom purge and trap preparation system following conversion to N_2O using the denitrifier method (Sigman et al. 2001; Casciotti et al. 2002), with nitrite removed by sulfamic acid addition (Granger et al. 2006). Values were corrected for size linearity and drift by regular analysis of international standards (USGS 32, USGS 34, and USGS 35), which were also used to normalize values to N_2 (for $\delta^{15}N$) and to vienna standard mean ocean water (VSMOW) (for $\delta^{18}O$). Typical error for $\delta^{15}N_{NO3}$ and $\delta^{18}O_{NO3}$ on duplicate measurements of the same nitrate sample was 0.2‰, which was similar to the 0.3‰ precision of internal quality control nitrate standards.

Nitrate isotope-based nitrification model

The dual isotopes of nitrate, $\delta^{15}N_{NO3}$ and $\delta^{18}O_{NO3}$, can be used to examine nitrogen transformations (Sigman et al. 2010; Casciotti 2016). In particular, by comparing to an established source signature, the concurrent variability of these isotopic signatures can be used to identify upper ocean N transformation processes such as nitrification. This deviation of the individual isotope's signature from the respective source nitrate isotope signature can be expressed as Δ(15,18), as presented in Sigman et al. (2005), and is calculated as:

$$\Delta(15,18) = \left(\delta^{15}N_{NO3\_measured} - \delta^{15}N_{NO3\_source}\right) - \left(\frac{^{15}\varepsilon_p}{^{18}\varepsilon_p}\right) * \left(\delta^{18}O_{NO3\_measured} - \delta^{18}O_{NO3\_source}\right) \quad (1)$$

where $\delta^{15}N_{NO3}$ and $\delta^{18}O_{NO3}$ are the stable isotope compositions of N and O in nitrate, respectively; source $\delta^{15}N_{NO3}$ and $\delta^{18}O_{NO3}$ values are assigned to the remnant mixed layer (RML) reference depth for each profile (as described in the "Results" section); $^{15}\varepsilon_p$ and $^{18}\varepsilon_p$ are the fractionation factors associated with NO_3^- assimilation by phytoplankton, where an $^{15}\varepsilon_p$:$^{18}\varepsilon_p$ of 1.0 is used in the present study (see below).

Incubation studies with phytoplankton have found $^{15}\varepsilon_p$:$^{18}\varepsilon_p$ to be very close to 1.0 (Granger et al. 2004, 2010). Phytoplankton exhibiting this behavior included *Thalassiosira* sp., *Emiliania huxleyi*, *Pseudo-nitzschia hemii*, *Phaeodactylum tricornutum*, and two *Synechococcus* species. If $^{15}\varepsilon_p$:$^{18}\varepsilon_p$ ~ 1.0, then according to Eq. 1 partial nitrate assimilation would produce $\delta^{15}N_{NO3}$ and $\delta^{18}O_{NO3}$ values that fall along a 1:1 line in a plot of $\delta^{15}N_{NO3}$ vs. $\delta^{18}O_{NO3}$, and Δ(15,18) would be ~ 0.0 (Sigman et al. 2005). Any deviation of Δ(15,18) from 0.0 would indicate either an unexpected assimilation $^{15}\varepsilon_p$:$^{18}\varepsilon_p$ or other N cycle processes occurring in the EZ.

Based on the assumption that negative Δ(15,18) values reflect EZ nitrification (Wankel et al. 2007; Fawcett et al. 2015; Rafter and Sigman 2016; Peng et al. 2018), Δ(15,18) calculated from Eq. 1, can then be used to estimate the proportional contribution of EZ nitrification to phytoplankton nitrate uptake according to the following equation developed in Wankel et al. (2007):

$$\Delta(15,18) = f_n * \left(\varepsilon_p - f_a * f_w * (\varepsilon_{ntr} - \varepsilon_a)\right) - \left(\frac{\delta^{18}O_{source} - \delta^{18}O_{source} * f_w + (\varepsilon_p * f_n) + (\delta^{18}O_{ntr} * f_n * f_w)}{1 - f_w + (f_n * f_w)}\right) + \delta^{18}O_{source}, \quad (2)$$

where f_n is the fraction of NO_3^- remaining relative to the source NO_3^-, ε_p is the fractionation factor for phytoplankton uptake of nitrate (determined for these samples as detailed in the following section), f_a is the fraction of ammonia assimilated by phytoplankton, f_w is the fraction of assimilated nitrate contributed by EZ nitrification, ε_{ntr} is the net isotope effect of ammonia and nitrite oxidation, ε_a is the isotope effect of ammonia assimilation, and $\delta^{18}O_{ntr}$ is the $\delta^{18}O$ of NO_3^- resulting from nitrification.

Cycle-specific fractionation factors for nitrate uptake (ε_p) were identified by carrying out a Rayleigh model fitting exercise (Supporting Information Fig. S1; e.g., Sigman et al. 2010). In this case, the ε_p was varied and source $\delta^{15}N_{NO3}$ and NO_3^- were kept constant to identify the ε_p that resulted in the lowest mean absolute difference between predicted and observed $\delta^{15}N_{NO3}$ values for each Cycle (*see* Supporting Information Text S1 for further details). Source $\delta^{15}N_{NO3}$ and NO_3^- were estimated to be associated with winter mixed layer

depths as will be described in further detail in the "Results" section below.

Suspended particulate organic matter collection and analysis

Seawater for suspended particulate organic matter (POM) isolation was collected from Niskin bottles into acid-washed Nalgene bottles. Between 1 and 2 L of seawater was immediately filtered under low vacuum (< 50 mm Hg) onto precombusted GF/F filters (25 mm, Whatman; nominal pore size of 0.7 μm). The volume filtered depended on Chl *a* and the sampling location. At the end of the filtration, each filter was wrapped in precombusted foil, placed inside sealed Whirlpak bags, and stored at −80°C until further processing. Inorganic carbon was removed by acidifying the filters with HCl vapor, followed by oven drying, overnight. One-half of the filter was used for PON and particulate organic carbon (POC) analysis on a Costech Elemental Analyzer (Costech Analytical Technologies, Valencia, CA, U.S.A.) according to standard protocols (*see* http://cce.lternet.edu/data/methods-manual).

Estimates of nitrate-based production

Nitrate "assimilation" rates for CCE cruises P1408 and P1604 were estimated from depth profiles of NO_3^- as previously developed for the CalCOFI grid (similar in form to that presented in Stephens et al. 2018). The NO_3^- supplied to the EZ (source nitrate) was represented by RML NO_3^- (the N and O isotope signatures of this "source" reservoir were also used in Eqs. 1, 2). Mean EZ nitrate was then subtracted from this source concentration to determine the amount of nitrate utilized at each location, based on the premise that any nitrate less than the source represents a removal due to assimilation. In order to then convert the stock of nitrate removed into a rate, we assumed that nitrate was assimilated by EZ organisms at the same rate as it was supplied by vertical advection from the RML (e.g., steady state). This assumption was evaluated in Stephens et al. (2018) and shown to be appropriate for this system. Nitrate supply was based on model-derived vertical advection rates (w) as obtained from the California State Estimate (located at http://sose.ucsd.edu/CASE/). Advection rates were averaged over ± 10 m surrounding the source depth, and ± 10 d and ± 20 km within sampling time and location, respectively.

Multiple linear regression analysis

A forward stepwise multiple linear regression analysis (MLRA) was performed on the long-term California Cooperative Oceanic Fisheries Investigations (CalCOFI) data set from stations nearest the CCE Cycles. These CalCOFI stations were classified as "Inshore" (lines 076.0 and 080.0, and Sta. 055.0 and 060.0) and "Midshore" (lines 076.0 and 080.0, and Sta. 070.0 and 080.0), similar to the regions classified in Fig. 1. A table of variables tested in the stepwise regression analysis is presented in Supporting Information Table S1, and Text S2 includes further details about the MLRA analysis.

Estimating *f*-ratio and nitrate uptake rates

To provide further context to the long-term CalCOFI data set, quarterly measurements of NH_4^+, NO_2^-, and NO_3^- between 2008 and the present were used to calculate an *f*-ratio after Harrison et al. (1987):

$$f-\text{ratio} = m\frac{NO_3}{(NO_3+NH_4)} + b, \quad (3)$$

where $m = 0.77 \pm 0.10$ and $b = 0.06 \pm 0.02$ as determined for the Southern California Bight. However, an *f*-ratio calculated in this way does not provide a nitrate uptake rate (i.e., a new production rate), and a new production rate estimate is needed to compare with f_w in Eq. 2 above, which is the proportion of nitrate uptake by phytoplankton that is derived from nitrification. To facilitate such a comparison, we first determined the satellite-based rate of net primary production (NPP) (VGPM model adjusted for the California Current; Kahru et al. 2009), and since the *f*-ratio represents the fraction of NPP that is derived from new/nitrate-based production, we could then calculate a rate of nitrate uptake by multiplying satellite NPP by the *f*-ratio from Harrison et al. (1987).

Results

Cruise and cycle context

As is typical for CCE process cruises, each Cycle of the P1408 and P1604 cruises followed particular water masses as determined by surface salinity, temperature, and Chl *a* (e.g., Landry et al. 2009; Goericke and Ohman 2015). Surface water (10–50 m) was anomalously warm by 0.8–1.5°C for all cycles during these two cruises (Zaba and Rudnick 2016). P1408 occurred just after the onset of the anomalous warming of surface waters in the California Current region, which may have been mediated by the encroachment of the North Pacific warm pool from the northwest into the CCE (Bond et al. 2015; Zaba and Rudnick 2016). P1604 caught the tail end of a strong El Niño and, at that time, the CCE was still a system in recovery from the warm anomaly (Jacox et al. 2016). As indicated by Fig. 1, Cycles 1, 2, and 3 during P1408 and Cycles 3 and 4 during P1604 were within the shelf break and were grouped as Inshore Cycles. Of the Inshore Cycles, P1408 Cycle 1 and P1604 Cycle 4 were the most productive as indicated by Chl *a* (Fig. 2) and ^{14}C-NPP rates (not shown).

During P1408, NO_3^- was nearly undetectable for most surface depths (0–80 m; Fig. 2). Surface mean (10–50 m) NO_3^- was ~ 4 μmol L^{-1} lower than the long-term average (1990–2016) for summer months at regional CalCOFI stations (determined for CalCOFI stations < 75 km of Pt. Conception; Supporting Information Fig. S3). Anomalously high NO_2^- (defined for NO_2^- and other variables as $>+1\sigma$ over the long-term CalCOFI mean) at the PNM was also observed for Inshore Cycles 1–3 during P1408 (Fig. 2), increasing up to about double the CalCOFI summer average (0.50 vs. 0.25 μmol L^{-1};

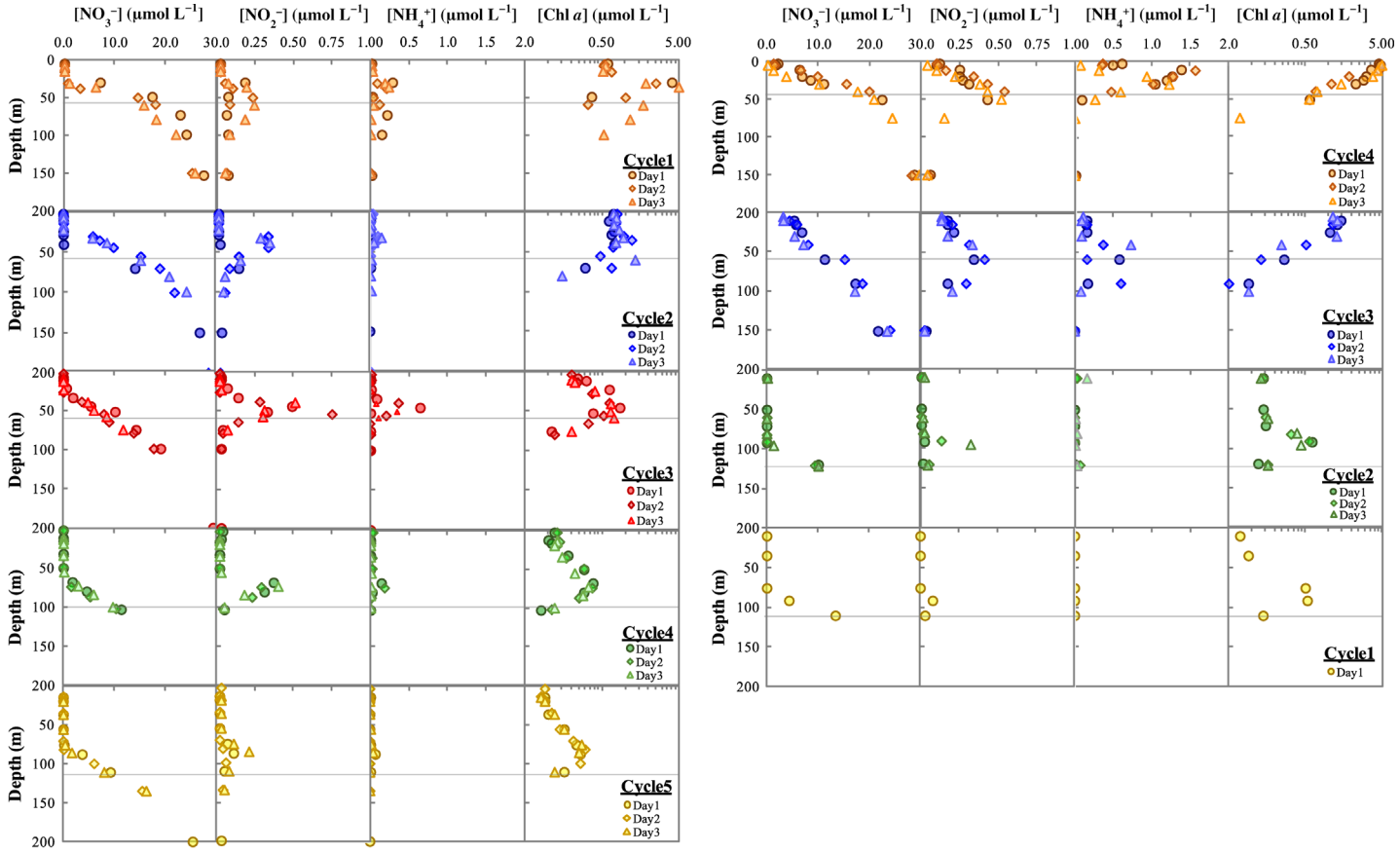

Fig. 2. CCE cruise P1408 (left) and P1604 (right) profiles of NO_3^-, NH_4^+, NO_2^-, and Chl *a*. Note the relative increase in NO_2^- for Cycle 3 P1408 and Cycle 4 P1604. The horizontal gray line inside each set of figures denotes the RML depth.

Supporting Information Fig. S4). P1604 Inshore Cycles 3 and 4 had higher surface NO_3^- (10–50 m) relative to Inshore Cycles sampled during P1408, but seasonal mean surface NO_3^- for P1604 was still 3–5 μmol L^{-1} less than the long-term mean spring values. Observations of low surface NO_3^- during the 2014 and 2016 sampling periods were consistent with enhanced surface stratification associated with warming (Jacox et al. 2016; Zaba and Rudnick 2016). At Inshore Cycles 3 and 4 of P1604, maximum NH_4^+ and NO_2^- were also nearly double that of the long-term spring mean concentration (1.0 vs. 0.5 μmol L^{-1} and 0.4 vs. 0.2 μmol L^{-1}, respectively; Supporting Information Fig. S4). Despite low NO_3^- and anomalously warm temperatures at the surface during 2014–2016, mean surface Chl *a* was not anomalously low in any region sampled by CCE-LTER cruises (Supporting Information Fig. S3).

Isotope signature of upwelling nitrate

EZ nitrification was estimated here from Δ(15,18) (Eq. 1; Wankel et al. 2007). To calculate Δ(15,18), the N and O isotope composition of nitrate at the surface and in source waters must be determined. We found that the characteristics of nitrate upwelling into the surface from the "remnant mixed layer" were most representative of source waters based on salinity and nitrate departures (Supporting Information Fig. S5). The RML usually identifies winter mixed layer waters that remain near the base of the spring and summer mixed layers that form during restratification and is a distinct layer based on salinity (and density) from the waters found deeper below (Cole et al. 2010).

During CCE cruises P1408 and P1604, the density at the base of the RML was between 25.3 ± 0.1 and 25.9 ± 0.1 kg m^{-3} (Supporting Information Table S2; *see* Supporting Information Text S3 for further details on how this was determined) and was comparable to previous RML estimates for the eastern North Pacific (25.4 kg m^{-3}; Cole et al. 2010). In this layer, NO_3^- was between 8.5 ± 2.0 μmol L^{-1} (P1408 Cycle 4, an Offshore Cycle) and 23.5 ± 2.7 μmol L^{-1} (P1604 Cycle 4, an Inshore Cycle; Table 1 and Supporting Information Fig. S5). For most Cycles, RML NO_3^- was between 14 and 17 μmol L^{-1}. The higher density and NO_3^- detected at the base of the RML during P1604 Cycle 4 (25.9 kg m^{-3} and 23.5 μmol L^{-1}, respectively) indicated enhanced upwelling conditions and the potential influence of a more saline, deeper, water mass.

Table 1. Integrated nitrate uptake estimates were used to convert f_w into EZ nitrification rates. Nitrification rates were estimated by multiplying calculated nitrate uptake rates by the fraction of nitrate uptake derived from nitrification ($f_{w,}$ Fig. 4). Vertical velocities (w) were determined based on the California State Estimate for ± 10 m around the source depth for ± 10 d surrounding Cycle locations. Standard deviations for these values were calculated based on this temporal and spatial variability. Standard deviations for other terms represent ± 1σ over the 2–4 d of each cycle. If w exhibited negative values (downwelling conditions), then nitrate uptake rates were negative, and so, nitrification rates were not estimated from the transport-based method.

Cruise	Cycle	Remnant MLD (m)	$[NO_3^-]$ at remnant MLD (μmol L^{-1})	$[NO_3^-]$ surface avg. (μmol L^{-1})	Source $\delta^{15}NO_3$ (‰)	w at remnant MLD (m d^{-1})	w-NO_3 uptake rate (mmol N m^{-2} d^{-1})	Integrated EZ nitrification rate (mmol N m^{-2} d^{-1})
P1408	1	60	17.6 ± 1.7	4.8 ± 0.9	8.5	0.18 ± 0.05	2.2 ± 0.2	0.47 ± 0.15
	2	60	14.1 ± 2.2	3.8 ± 2.0	9.0	0.18 ± 0.18	1.9 ± 0.2	0.33 ± 0.05
	3	60	10.0 ± 1.8	3.3 ± 0.7	9.5	0.39 ± 0.02	2.6 ± 0.6	0.93 ± 0.10
	4	100	8.5 ± 2.0	1.8 ± 0.5	9.3	0.31 ± 0.13	2.1 ± 0.5	0.46 ± 0.10
	5	115	10.1 ± 1.2	1.8 ± 0.6	9.4	0.29 ± 0.02	2.4 ± 0.2	—
P1604	1	110	12.7 ± 3.1	3.6 ± 0.9	8.6	–0.34 ± 0.13	—	—
	2	120	12.9 ± 3.9	2.7 ± 1.1	8.6	–0.06 ± 0.06	—	—
	3	55	12.9 ± 1.5	6.7 ± 1.2	8.9	0.30 ± 0.11	1.8 ± 0.3	0.34 ± 0.12
	4	50	23.5 ± 2.7	9.6 ± 1.8	8.7	0.58 ± 0.10	8.1 ± 0.7	2.07 ± 0.95

On average, $\delta^{15}N_{NO3}$ at RML source depths was 8.9 ± 0.4‰ (ranging between 8.5 and 9.5‰ for $NO_3^- < 25\,\mu$mol L^{-1}; Table 1 and Supporting Information Table S2), and was enriched by 1.1 ± 0.7‰ compared to waters immediately below (densities between 25.9–26.8 kg m^{-3} and NO_3^- between 22 and 40 μmol L^{-1}; n = 23; Supporting Information Text S3, Fig. S6). A mean RML source $\delta^{15}N_{NO3}$ value of ~8.9‰ is slightly elevated compared with previous reports for Monterey Bay—located slightly north of our study region (Altabet et al. 1999; Wankel et al. 2007; Santoro et al. 2010)—but follows isoscape source $\delta^{15}N_{NO3}$ estimated from compound-specific $\delta^{15}N$ amino acid analyses along the California margin (Vokhshoori and McCarthy 2014).

Isotope fractionation during nitrification

As NO_3^- decreased in the surface ocean for CCE cruises P1408 and P1604, $\delta^{15}N_{NO3}$ (shown in Fig. 3) and $\delta^{18}O_{NO3}$ (not shown but as indicated by concurrent isotopic enrichments in Supporting Information Fig. S7) increased as a result of isotope fractionation during nitrate uptake by phytoplankton (Sigman et al. 2010). However, $\delta^{18}O_{NO3}$ is further enriched during the incorporation of new O atoms that reflect the combined $\delta^{18}O$ of water (2/3rd) and O_2^- (1/3rd) (Buchwald et al. 2012; Casciotti 2016). Other processes that influence the $\delta^{18}O$ of nitrate include the isotope effects of nitrite oxidation and water incorporation as well as fractionation during the exchange of water atoms between NO_2^- and water (Buchwald and Casciotti 2010). Additionally, the $\delta^{15}N_{NO3}$ regenerated via nitrification introduces isotopically depleted N from the strongly fractionating process of NH_4^+ oxidation (relative to NH_4^+ assimilation). These combined processes acting on ^{15}N and ^{18}O during nitrification lead to a slight enrichment in ^{18}O relative to ^{15}N when compared to the source nitrate isotope signature. The additional enrichment in $\delta^{18}O_{NO3}$ that results from nitrification can be visualized as a positive offset from the $\delta^{18}O_{NO3}$:$\delta^{15}N_{NO3}$ = 1 slope in our data (Supporting Information Fig. S7). As shown in Eq. 1, such a positive offset results in negative values for Δ(15,18), which is emblematic of nitrification. Negative Δ(15,18) values were observed in the EZ for nearly all Cycles for the CCE cruises presented here (Fig. 3) and Inshore Cycles had the most negative values overall, which indicated that nitrification contributed strongly to N cycle processes in the EZ at these locations. However, the coarser sampling resolution in Midshore to Offshore Cycles may have masked isotopic deviations associated with EZ nitrification at those locations.

The profiles with more negative Δ(15,18) were also associated with greater predicted f_w, a value reflective of the percentage of assimilated nitrate derived from the combined steps of nitrification within the EZ (Fig. 3). In the model presented in Eq. 2, the parameters (ε_{ntr}, f_a, etc.) were held constant and f_w values were adjusted using a solver-based approach to minimize the difference between Δ(15,18) estimated from Eq. 1 and Δ(15,18) calculated from Eq. 2. As discussed in Wankel et al. (2007), the model is sensitive to the values selected for both $\delta^{18}O_{NO3}$ resulting directly from nitrification ($\delta^{18}O_{ntr}$) and the fraction of ammonia directly assimilated by phytoplankton (f_a). Model parameters in Eq. 2 were previously optimized for the central California Current in Wankel et al. (2007) using an iterative approach by testing the range of known and possible values. A similar approach was adopted here for the CCE region and the range in parameters that were tested are listed in Supporting Information Table S3. Profiles of f_w can be found in Fig. 3 and the median f_w (and 25th and

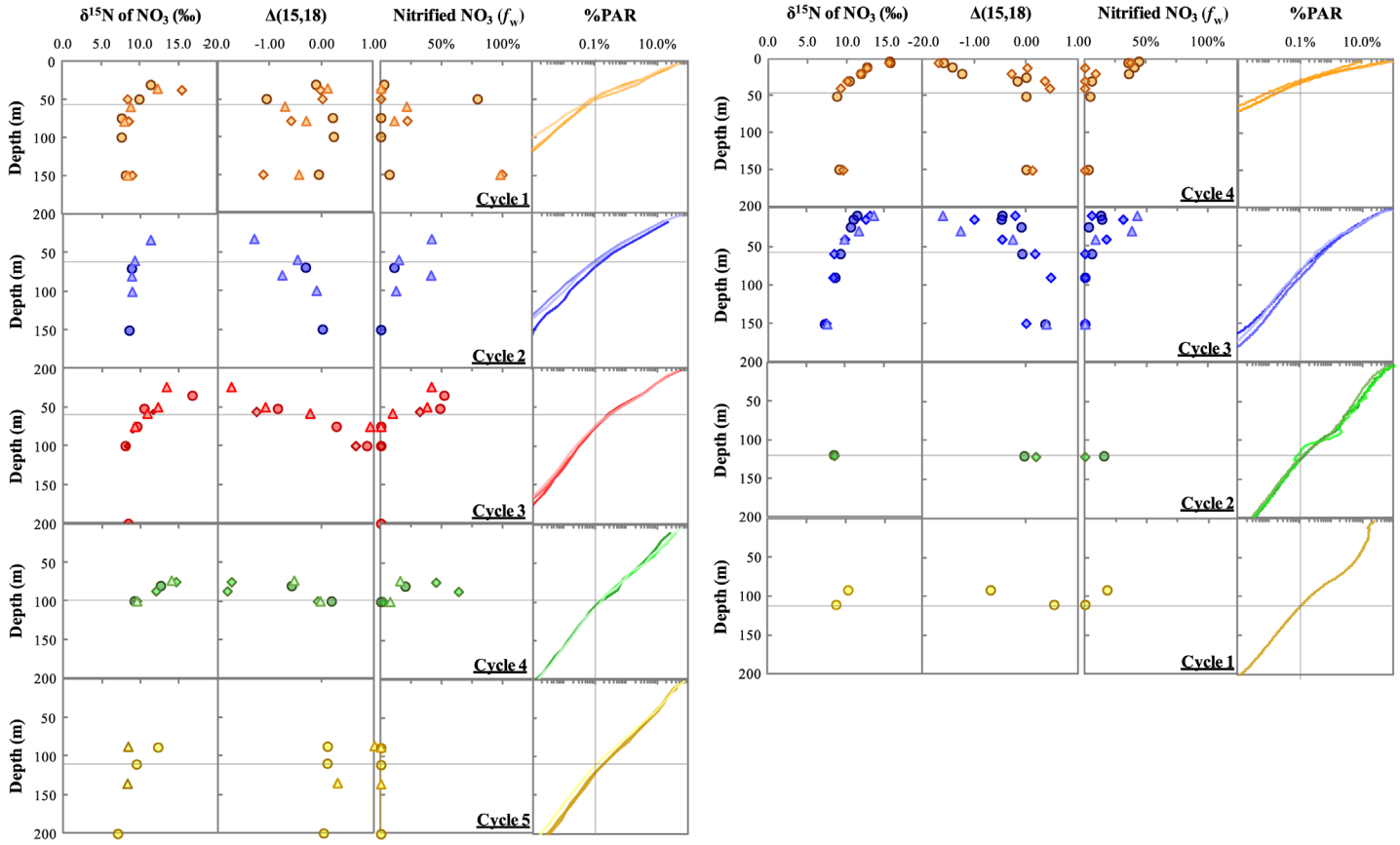

Fig. 3. Profiles of P1408 (left) and P1604 (right) $\delta^{15}N_{NO3}$, Δ(15,18), f_w (or the contribution of nitrification to nitrate uptake), and % surface PAR. Legends and the horizontal gray lines are the same as for Fig. 2. The vertical gray line in the %PAR figures represents the 0.1% light level. Model parameters used to estimate f_w in this figure represented a range of tested parameters as can be found in Supporting Information Table S1.

75th percentile values) from the combined range of tested parameters (26 model iterations) is shown in Fig. 4.

Median EZ nitrification contributions to incorporated nitrate (f_w) varied from 6% to 36%, with most Cycles falling between 15% and 23% (Fig. 4 and Supporting Information Table S4). The average of these f_w values for the CCE is similar to the average f_w values (15–27%) reported for the Monterey Bay (Wankel et al. 2007). A correspondence between the values previously estimated and those estimated here is not surprising given that the range in tested parameters and observed Δ(15,18) values were relatively similar between these sites, though the model parameters tested here were slightly more constrained by recent contributions from related studies (e.g., Casciotti 2009; Sugimoto et al. 2009; Buchwald and Casciotti 2010; Santoro and Casciotti 2011; Buchwald et al. 2012). For each Cycle, the 25th and 75th percentile values for f_w were on average 6–8% away from the median. After accounting for the significant range among tested model parameters, f_w values for P1408 Cycle 3 and P1604 Cycle 4 were significantly greater (and significantly less for P1604 Cycle 2; Mann–Whitney, $p < 0.01$) than values for all other Cycles.

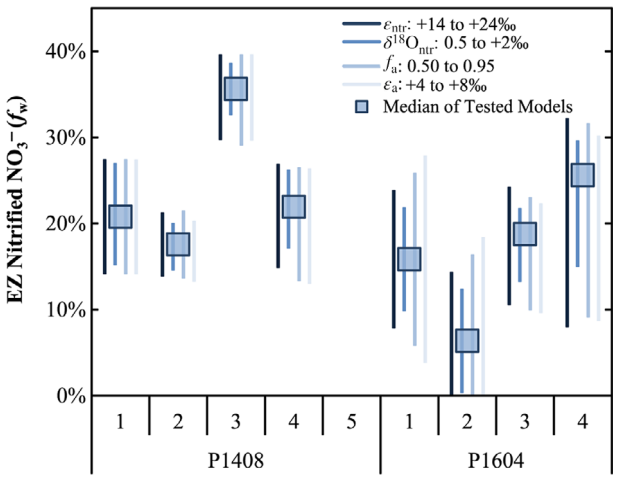

Fig. 4. Model parameters were tested by comparing integrated %nitrification, where the square symbol represents the median f_w derived from all tested parameters (n = 26 model variations). The length of the line extends from the 25th to the 75th percentile value for each tested parameter. No data are shown for P1408 Cycle 5 as there was no EZ detection of negative Δ(15,18) for this Cycle (as shown in Fig. 3).

AOA is widespread (Santoro et al. 2018) and the isotope effect for AOA played an important role in the isotope model here, where previous estimates found the AOA isotope effect to be 22 ± 5‰ (Santoro and Casciotti 2011). The f_w model is particularly sensitive to the difference (though not to the absolute values) between isotope effects associated with the combined steps of nitrification ($^{15}\varepsilon_{ntr}$) and ammonia assimilation ($^{15}\varepsilon_a$). Empirical determinations of $^{15}\varepsilon_a$ have also indicated preferential uptake of the lighter ammonium isotope, with $^{15}\varepsilon_a > +6‰$ (e.g., Montoya et al. 1991). The second step in nitrification is carried out by NOB, and cultured and field populations have a unique inverse isotope effect between −9 ± 2‰ and −20 ± 3‰ (Buchwald and Casciotti 2010). The combined net isotope effect of nitrification (i.e., $^{15}\varepsilon_{ntr}$) could theoretically be between +2 and +22‰, but $^{15}\varepsilon_{ntr} < +14‰$ did not yield any viable model solutions. Additionally, the dependence of model solutions on $^{15}\varepsilon_{ntr} > +14‰$ is consistent with field studies of Sugimoto et al. (2009) (20 ± 5‰) and the optimized values in the model of Wankel et al. (2007) (+19‰). Finally, it should also be noted that possible variations in the isotope effect of nitrate uptake ($^{15}\varepsilon_p$) had little effect on modeled f_w. For example, use of a typical open ocean $^{15}\varepsilon_p$ of +5‰ (Sigman et al. 1999; Altabet 2001) instead of the ~ +3‰ estimated here (Supporting Information Text S1 and Fig. S1) only decreased the model estimated median EZ f_w by 2%, on average.

Nitrification rates and evidence of ammonia oxidation

The estimated 6–36% median contribution of EZ nitrification to NO_3^- (Fig. 4) provided by the dual isotope method refers only to the proportion of assimilated NO_3^- contributed by the combined steps of nitrification and provides no information on the rates and magnitudes of ammonia and/or nitrite oxidation. However, if nitrate uptake rates are known, then the rates of the combined steps of nitrification can be inferred by multiplying the nitrate uptake rate by the f_w parameter (Table 1). Depth-integrated assimilation rates were estimated by multiplying the EZ NO_3^- deficit by vertical advection rates (as previously employed for the California Current in Stephens et al. 2018). Assimilation rates estimated in this manner ranged from 1.8 to 8.1 mmol N m^{-2} d^{-1} (Table 1). Multiplying median f_w values (Supporting Information - Table S4) by these nitrate assimilation rates resulted in integrated EZ (down to RML depths) nitrification rates of 0.33 ± 0.05 to 2.07 ± 0.95 mmol N m^{-2} d^{-1} (Table 1). During P1604, the nitrate uptake rates could not be estimated at two of the four Cycles because vertical transport values at these two sites were negative (i.e., net downwelling), which implied that no new NO_3^- was transported by vertical advection into the surface at that time.

To provide additional context to our geochemical measurements, we used 16S rRNA gene sequencing and detection of *amoA* transcripts collected during P1604 to determine whether the dominant organisms (AOA) and genes (archaeal *amoA*) regulating the first and rate-limiting step of nitrification, ammonia oxidation, were present and active throughout the water column (Supporting Information Text S4 and Fig. S8). In general, AOA 16S rRNA and *amoA* displayed an expected increase with depth; however, *amoA* expression was detected in the EZ for P1604 Cycle 4 and to a lesser extent Cycle 3. P1604 Cycles 3 and 4 also had higher than average NH_4^+ and NO_2^- throughout the EZ (Supporting Information Fig. S4), providing further evidence that sufficient substrates were present for both steps of nitrification to have been occurring throughout the EZ for these Cycles.

Discussion

Aerobic nitrification is an essential process in the oxidation of inorganic nutrients to nitrate. Many studies along the California margin have shown that nitrification is largely restricted to regions in the water column with low light levels (Ward et al. 1984; Ward 1985; Santoro and Casciotti 2011). Yet, both components of nitrification, ammonia and nitrite oxidation, have been detected in the EZ extending up to surface depths (Ward 1987, 2005, 2008; Ward et al. 1989; Dore and Karl 1996; Smith et al. 2016). The location of nitrification is particularly relevant to evaluating the role of "new" vs. "recycled" nitrate in supporting primary production and examining the *f*-ratio (e.g., Dugdale and Goering 1967; Eppley and Peterson 1979). Nitrification has been previously studied in the CCE during more climatologically neutral years and has been studied based on either the isotope approach (Wankel et al. 2007) or rate determinations from incubations and gene transcript abundances (Ward 1987, 2005, 2008; Ward et al. 1989; Santoro et al. 2010, 2013; Smith et al. 2016). In this study, we have primarily used the isotopes of nitrate to quantify EZ nitrification during two anomalously warm years in the CCE.

Evidence for nitrification

Negative Δ(15,18) values observed in near-surface, oxygenated waters have been attributed to surface ocean nitrification (Fawcett et al. 2015; Rafter and Sigman 2016; Peng et al. 2018). These negative Δ(15,18) excursions have been previously detected in surface waters near Monterey Bay (Wankel et al. 2007) and the Antarctic Zone (Fripiat et al. 2015; Smart et al. 2015). However, negative Δ(15,18) values were rare in the EZ of more open ocean sites such as the Equatorial Pacific (Rafter and Sigman 2016), Sargasso Sea (Fawcett et al. 2015) and the subarctic North Atlantic (Peng et al. 2018). Our isotope data indicated that EZ nitrate in the CCE at this time was being influenced by nitrate assimilation (based on an increase in both $\delta^{18}O_{NO3}$ and $\delta^{15}N_{NO3}$) and nitrification (based on the observed negative Δ(15,18); Fig. 3).

Regions of enhanced contributions of EZ nitrification to surface nitrate (f_w) corresponded with EZ NH_4^+ and NO_2^- that were greater than the long-term mean (Supporting Information Fig. S4), and a subset of the data set were associated

with EZ detection of *amoA* gene transcripts (P1604 Cycles 3 and 4; Supporting Information Text S4 and Fig. S8). Gene transcripts were used here as a proxy for the activity of the enzyme that catalyzes ammonia oxidation to nitrite, the first step of nitrification. Correspondence between *amoA* gene transcripts and f_w in the EZ for some Cycles indicated that, at times, nitrite production through ammonia oxidation was spatially coupled to nitrate production (via the combined nitrification steps based on nitrate isotopes). For other Cycles, the lack of correspondence suggested that ammonia and nitrite oxidation were temporally decoupled (Ward 1987), either because the isotope signature of nitrification observed in the EZ was a relict feature or because nitrite produced elsewhere was supplied to the EZ and subsequently oxidized there.

Previous studies have suggested that *amoA* transcripts (Church et al. 2010; Smith et al. 2014*a*) or *amoA* gene copies (Beman et al. 2008) reflect active ammonia oxidation and can be correlated with ^{15}N oxidation rates (Beman et al. 2008), whereas the geochemical signature of nitrification can include a remnant feature associated with nitrification elsewhere in the water column or water mass (e.g., Fripiat et al. 2015). For instance, an isotope model for the Southern Ocean demonstrated that wind-driven mixing displaced the geochemical memory of nitrification taking place just below the EZ to shallower depths (Fripiat et al. 2015). Such a memory effect is further consistent with the relatively long timescale of influence recorded by the isotope signature of nitrate (as highlighted for the subarctic North Atlantic in Peng et al. 2018). When *amoA* gene transcripts and geochemical measurements overlap (Supporting Information Fig. S8), we may be able to more confidently attribute f_w to an active, local process.

Physical transport of isotope signature

To test whether negative Δ(15,18) values observed in the CCE were being vertically advected upward through the EZ following nitrification in deeper waters, we constructed a simple three-box model for cycles of P1604, where both *amoA* gene copies and Δ(15,18) were available (Supporting Information Fig. S8). The water column was divided into three light regimes: (1) surface to 5% PAR, (2) 5% to 1% PAR and (3) 1% PAR to the RML depth. The model assumed that lateral mixing (e.g., salt fingering described in Todd et al. 2012 for the CCE) was minimal (Supporting Information Fig. S5) and that negative Δ(15,18) values were either from local nitrification or upward transport of the isotope signature of nitrification from the deeper box into the depth of interest.

Once we established the subeuphotic f_w that was advected upward (RML f_w values in Fig. 5), the local nitrification rate within each box was estimated based on the concentration of NO_3^-, the vertical transport rate, and the local f_w for that box. At both Cycles 3 and 4 during P1604, we found that local nitrification (*see* Fig. 5, light bar) exceeded advected f_w (dark bar in Fig. 5; $p < 0.01$, Mann–Whitney). The upward increase in the proportion of nitrified NO_3^- utilized by phytoplankton (i.e., f_w) cannot be attributed to either preferential vertical transport or preferential phytoplankton uptake of nitrified NO_3^-, and so, must be supported by local nitrification.

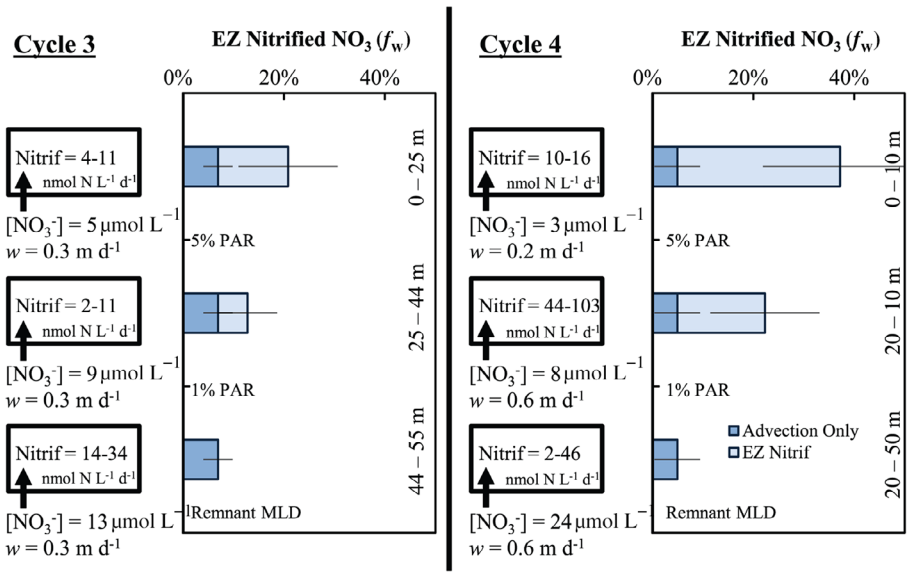

Fig. 5. The relative contribution of (1) the nitrification signal transported from the remnant mixed layer depth (MLD) by advection (darker colored bars) and (2) local nitrification (lighter colored bars), to f_w determined for P1604 Cycles 3 and 4 from Eq. 2. Nitrification rates are presented within the boxes to the left of each chart and were estimated based on multiplying f_w values by vertical nitrate transport (from *w* and nitrate concentration data) into the boxes. Because the source nitrate for the f_w-based approach is at the RML depth, typically located above the 0.1% PAR level (Figs. 2, 3), any f_w observed above this would be associated with local nitrification.

The estimated nitrification rates for surface waters (0 m) to 1% PAR boxes (2–103 nmol N L^{-1} d^{-1}; Fig. 5) encompassed the range of published values for comparable light regimes in the central California Current (2–80 nmol N L^{-1} d^{-1}; Ward et al. 1982; Santoro et al. 2010; Smith et al. 2014*a*,*b*, 2016). At these NO_2^- concentrations, albeit under reduced oxygen content, nitrite oxidation rates have been published that are comparable to those we have estimated here (Fig. 5) (Sun et al. 2017). During P1604, the boxes where greater rates of upper EZ nitrification were estimated corresponded well to locations where *amoA* gene copies were detected (P1604 Cycle 4; Supporting Information Text S4 and Fig. S8).

Processes influencing nitrification in the southern California Current System

In order to place our CCE data into a broader context, we used a linear correlation analysis to identify water column properties that covaried with the range of EZ nitrification contributions (f_w) we observed for our study. We examined the suite of chemical data available through the CCE LTER program (http://cce.lternet.edu/) and tested either depth integrated values, surface mean (~ 0–50 m) values or values from primary maxima. A significant correlation ($r^2 = 0.81$, $p < 0.01$) with f_w was only observed for NO_2^- at the PNM (Fig. 6). Prior studies have demonstrated that ammonia oxidation rates in the California Current can be positively correlated with NH_4^+ concentrations (Smith et al. 2014*b*), and further south in the eastern tropical North Pacific, NO_2^- and nitrite oxidation rates were closely coupled (Beman et al. 2013). The stronger positive correlation between median f_w and PNM NO_2^- here suggests that the temporal imprint of nitrification on NO_3^- isotopes is closely coupled to the availability of NO_2^-. In the CCE, it is possible that high PNM NO_2^- concentrations supply NO_2^- to the upper EZ during upwelling and Ekman pumping, which in turn can drive enhanced EZ nitrification.

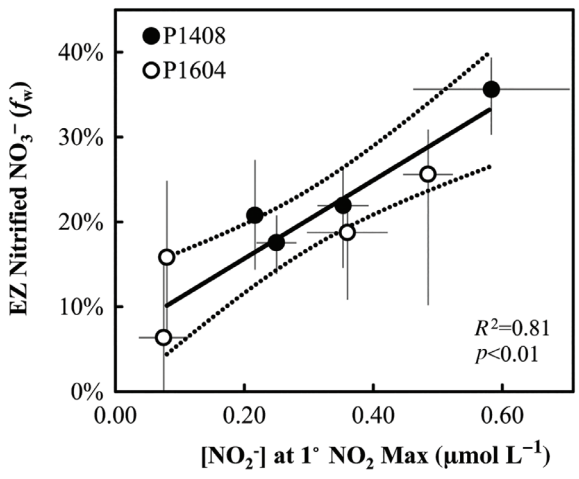

Fig. 6. Median EZ nitrified nitrate (f_w) vs. NO_2^- concentrations at the depth of the PNM concentrations. Error bars for NO_2^- represent $\pm 1\sigma$ across the Cycle days and for f_w represent the 25th and 75th quartiles across the days and 26 model variations. The best fit line in bold was calculated using a Type II linear fit and the dotted lines surrounding the best fit line are the ± 95% confidence intervals.

Long-term nitrite trends in CalCOFI

Interpreting the linear relationship in Fig. 6 as a predictive relationship, where the concentration of NO_2^- at the PNM is used to estimate variations in EZ nitrification, we identify the frequency of periods of enhanced PNM NO_2^-. By extending this relationship, we used NO_2^- measured as part of the long-term California Cooperative Oceanic Fisheries Investigations (CalCOFI) Program to infer relative interannual variability in nitrification in the southern CCS. Quarterly NO_2^- profiles have been measured from CalCOFI's ~ 72 stations since the mid-1980s, and we isolated the stations nearest the CCE study region presented here. This data set showed that NO_2^- at the PNM averaged 0.29 ± 0.10 μmol L^{-1} for both Inshore and Midshore regions but that the Midshore exhibited greater variability (up to 1.2 μmol L^{-1} at times; Fig. 7). During 11 and 19 cruises, in the Inshore and Midshore regions, respectively, NO_2^- exceeded 0.41 μmol L^{-1} (i.e., $+1\sigma$; out of the ~ 106 cruises presented in Fig. 7). The majority (> 60%) of events with elevated NO_2^- occurred during summer cruises (noted as red diamonds in Fig. 7). NO_2^- events in excess of 0.64 μmol L^{-1} (or $+3\sigma$) were only observed in the Midshore region and occurred primarily surrounding strong El Niño Southern Oscillation (ENSO) events (e.g., 1991, 1999, and 2016), though this climatological pattern was not consistent for all high NO_2^- events (e.g., 2006).

Predicting influences of EZ nitrification on new production

Based on PNM NO_2^- values and the linear fit in Fig. 6, the calculated long-term mean f_w for both the Inshore and Midshore CalCOFI regions was $20\% \pm 6\%$ (Fig. 7). The mean CalCOFI EZ nitrification contribution is similar to global model estimates of 17% (Zakem et al. 2018) and confirms the relevance of the global value for a productive eastern boundary current system like the California Current. In the Inshore, f_w rarely exceeded 25% (11 cruises out of 107), whereas in the Midshore, f_w could surpass 30% (19 cruises out of 106). The estimated f_w represents the "extra" nitrate in the EZ derived from local nitrification and not externally supplied to the EZ by upwelling from below RML depths. Thus, EZ nitrification could potentially mislead our calculations of new production. To determine the extent to which new production estimates could be impacted, we first calculated *f*-ratios (after Harrison et al. 1987) from existing long-term data sets of inorganic N species (i.e., NO_3^-, NO_2^-, and NH_4^+) as measured by CalCOFI. The calculated mean *f*-ratios were 0.69 ± 0.09 and 0.56 ± 0.15 for cruises between 2008 and 2016 in the Inshore and Midshore region, respectively. To convert these *f*-ratios into nitrate uptake rates (new production rates), we used average satellite NPP for the Inshore and Midshore regions from the same time period

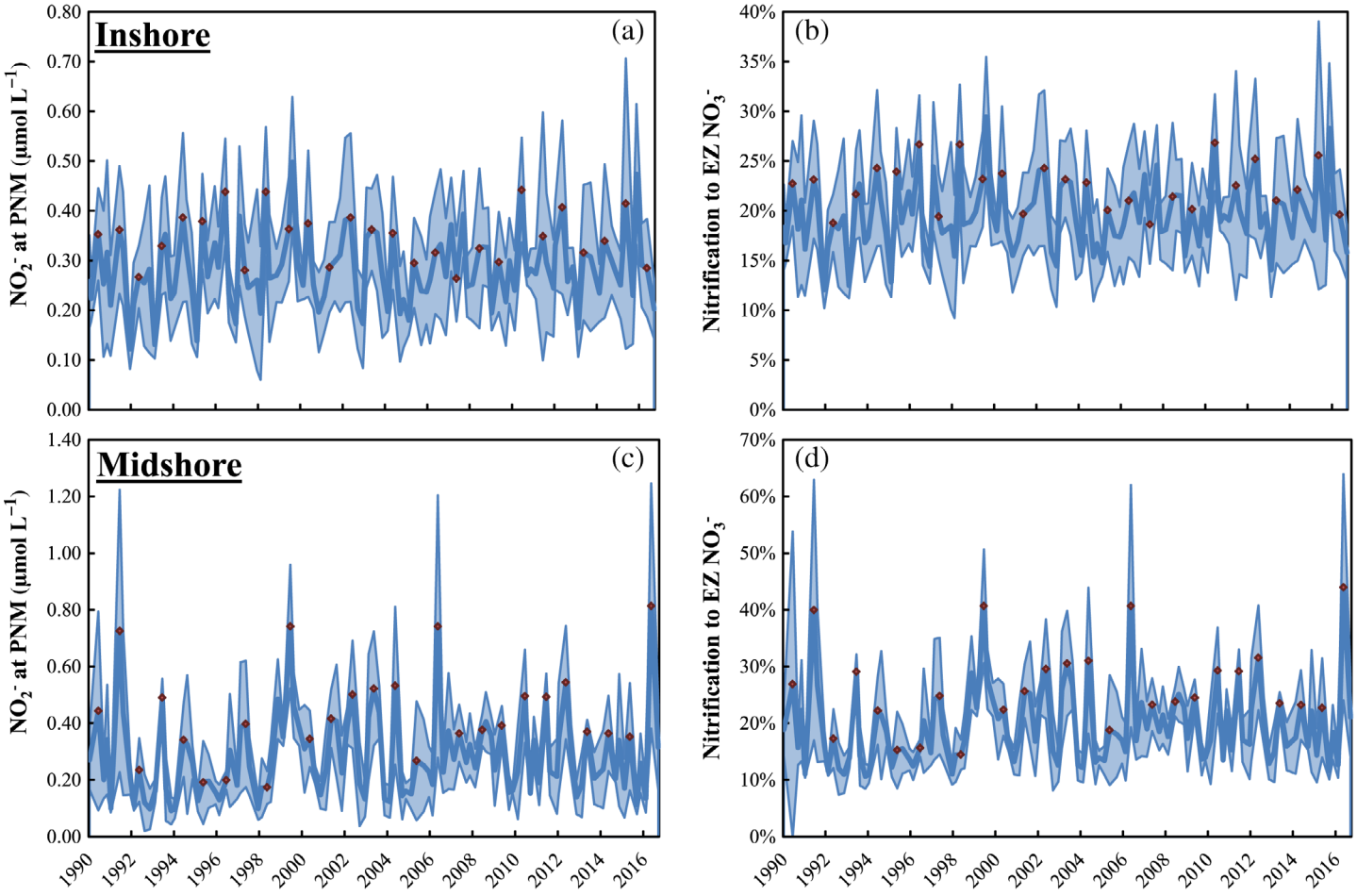

Fig. 7. CalCOFI time series of NO_2^- at the PNM depth (± 7 m) for Inshore (**a**) and Midshore (**c**) stations located nearest (< 50 km) P1408 and P1604 CCE Cycles (Fig. 1). The relationship between f_w and PNM NO_2^- in Fig. 6 was used to predict nitrification for Inshore (**b**) and Midshore regions (**d**). The error bands represent the standard deviations for each CalCOFI cruise (n = 4–7 stations per cruise). Red diamonds denote summer cruises (June–August).

(67 ± 37 mmol C m^{-2} d^{-1} and 31 ± 6 mmol C m^{-2} d^{-1}, respectively). Average nitrate uptake rates predicted in this manner were 47 ± 20 mmol C m^{-2} d^{-1} and 17 ± 8 mmol C m^{-2} d^{-1} for the Inshore and Midshore regions, respectively. The long-term mean f_w (20% ± 6%) for each region was then used with estimated total nitrate uptake to calculate an average "true" new production rate: 38 ± 16 mmol C m^{-2} d^{-1} and 14 ± 6 mmol C m^{-2} d^{-1} for the Inshore and Midshore, respectively.

The supply of new nutrients incorporated by surface ocean biomass should balance the export out of the EZ for systems to remain in steady state over long time scales (Dugdale and Goering 1967; Eppley and Peterson 1979). However, even after adjusting for EZ nitrification, the estimated nitrate uptake rates and thus, new production rates (14–38 mmol C m^{-2} d^{-1}), exceeded annually averaged sinking export for the Inshore CCE region (3–20 mmol C m^{-2} d^{-1}, Altabet et al. 1999; Pennington et al. 2010; Collins et al. 2011; Stukel et al. 2011, 2017; Haskell et al. 2016). Accounting for EZ nitrification does bring new production and sinking export in closer agreement, but other explanations are needed to explain the remaining discrepancy between these two estimates. Some studies have suggested that the surface accumulation and subsequent subduction of nonsinking organic matter is an important pathway of additional export that returns new production to the dark ocean (Plattner et al. 2005; Stukel et al. 2018; Stephens et al. 2018).

PNM formation in the California Current

The majority of the > 25-yr CalCOFI record of PNM NO_2^- exhibited relatively low variability and was primarily characterized by seasonal dynamics (Fig. 7). As such, the positive excursions (> 0.41 µmol L^{-1} NO_2^-, or +1σ) were intriguing because the extremes might provide insight into the factors that strongly influence NO_2^- accumulation and thus nitrification. Factors contributing to NO_2^- accumulation in the surface ocean have been previously reviewed (e.g., Lomas and Lipschultz 2006), and several hypotheses have been offered for

the widespread recurrence of the PNM water column feature (e.g., Zakem et al. 2018).

The long-term CalCOFI data set was used to examine controls on NO_2^- and, by extension based on the observed CCE correlation (Fig. 6), on f_w. Using the long-term data (2004–2016) from the CalCOFI Program, a stepwise linear regression analysis was conducted with PNM NO_2^- as the predictor variable and was followed by an MLRA. Stepwise regression of 16 parameters (Supporting Information Table S1) ultimately isolated four predictors (listed here in order of importance based on Mallows' Cp, Supporting Information Fig. S2): mean PON (0–50 m), mean POC:Chl *a* (0–50 m), mean O_2 saturation (0–30 m), and the Multivariate ENSO Index. Of the four parameters, PON and POC:Chl *a* together accounted for the majority of the linear prediction (an adjusted R^2 = 24.3% for the two parameters compared to 30.0% by including all four parameters, both models with $p < 0.01$).

From the two best predictors from the MLRA, $NO_2^- > +1\sigma$ was typically associated with either high PON in the Inshore (four out of six cases for Inshore) or high POC:Chl *a* in the Midshore (9 out of 12 cases for Midshore, Fig. 8). Most of the stations with elevated PON were low in POC:Chl *a* (because Chl *a* was high) and vice versa (15 out of the 18 combined Inshore and Midshore stations). For CCE Cycles where NO_2^- was elevated ($> 0.40\ \mu mol\ L^{-1}$; Fig. 2), either high POC:Chl *a* (and low PON; P1408 Cycle 3) or high PON (P1604 Cycle 4) effectively predicted the high observed NO_2^-.

Based on these MLRA findings, we suggest that elevated PON provides a substrate for greater ammonia production by heterotrophic bacteria, zooplankton, or other organisms, which marks the beginning of the cascade of nitrification reactions that include the production of nitrite. In this scenario, there is sufficient inorganic nitrogen to support both phytoplankton and nitrifying archaea and bacteria (i.e., ammonia and nitrite oxidizers) within the EZ. Whereas when Chl *a* is low (i.e., when POC:Chl *a* is high), the competition from phytoplankton for ammonia and nitrite is reduced and nitrification rates can be elevated. Extending the MLRA further back in time (1990–2016, where POM data were not available) further supports the interpretation of reduced competition with phytoplankton where PNM NO_2^- was inversely correlated with integrated chlorophyll and dynamic height, among other variables (Supporting Information Table S5 and Fig. S9).

Both scenarios determined from the MLRA (increased POM substrate and reduced competition from phytoplankton) allow NO_2^- to accumulate as a substrate for nitrite oxidation leading to enhanced nitrifier activity. Such a pathway is supported by additional evidence that heterotrophic bacteria comprised a greater proportion of the upper ocean biomass when PNM NO_2^- exceeded the long-term mean (Supporting Information Fig. S10). Data from the time series (2004–2016) could also suggest an interconnection at times between Inshore and Offshore regions. For instance, Midshore 200607 and 201607 CalCOFI cruises had elevated NO_2^- but no local correlation with predicted parameters (Fig. 8). Instead, for these two cases of higher Midshore NO_2^-, we observed that Inshore PON was significantly elevated over the mean ($> 2.0\ \mu mol\ L^{-1}$) suggesting that excess PON could have been transported offshore contributing to NO_2^- in the Midshore (Stukel et al. 2018).

The observed relationship between PNM NO_2^- and f_w (Fig. 6) suggests that the proportion of EZ NO_3 that is derived

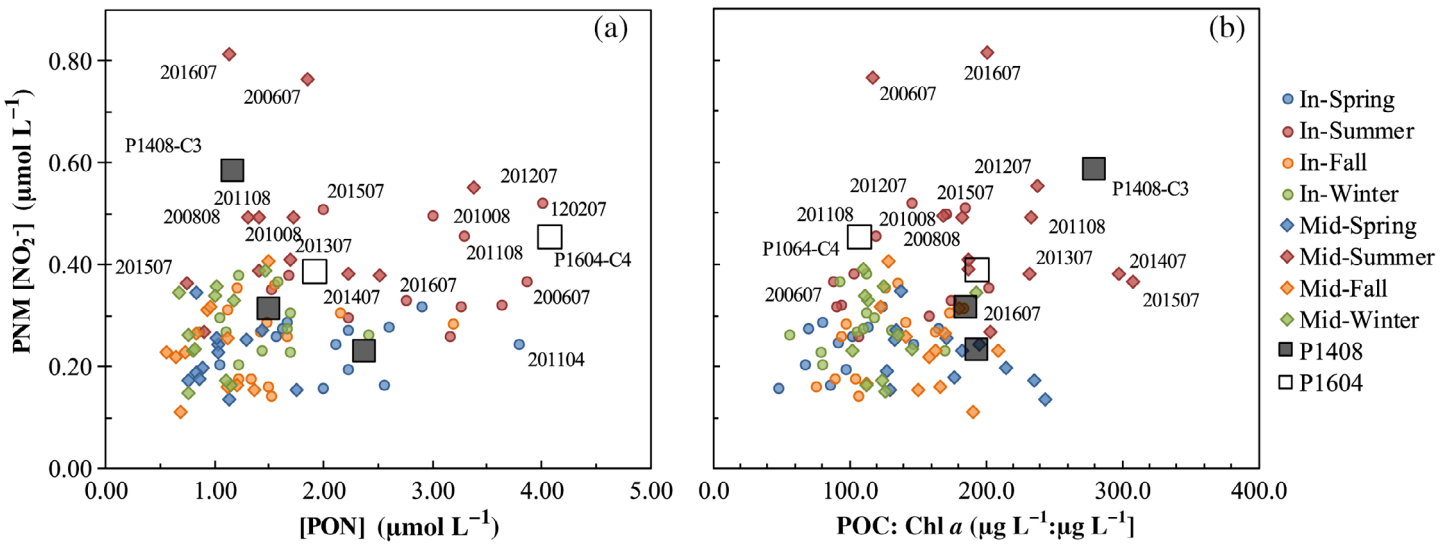

Fig. 8. The relationship of primary nitrite maximum (PNM) NO_2^- to PON (**a**) and POC:Chl *a* (**b**) is shown to highlight conditions leading to elevated $[NO_2^-]$ for CalCOFI stations and CCE Cycles. Data from CalCOFI 2004–2016 Inshore stations ("In"; Lines 076.0 and 080.0 and Sta. 055.0 and 060.0; circles) and Midshore stations ("Mid"; Lines 076.0 and 080.0 and Sta. 070.0 and 080.0; diamonds) were included in the analysis. Overlain are mean observed and predicted Inshore CCE cruise Cycles (large squares).

from EZ nitrification is primarily influenced by the extent of NO_2^- accumulation at the PNM. In our study, we find NH_4^+ to be similar to or exceed NO_2^- in most cases (Fig. 2 and Supporting Information Fig. S4); and the calculated affinity of ammonia oxidizers for NH_4^+ (Zakem et al. 2018) as well as the kinetics of oxidation (Martens-Habbena et al. 2009; Horak et al. 2013) indicates that observed concentrations are sufficient for ammonia oxidizers to supply nitrite. Thus, the production of NO_2^- observed here is likely linked to NH_4^+ oxidation as suggested previously for the California Current and not controlled by assimilatory NO_3^- reduction by light-limited phytoplankton (Santoro et al. 2013). The relationship between NO_2^- and f_w further indicates that both NO_2^- production at the PNM and removal are taking place. It has been shown that NOB have a relatively high NO_2^- requirement (Zakem et al. 2018) and higher half saturation constants (K_s) for NO_2^- oxidation (Sun et al. 2017) compared to ammonia oxidizers (Martens-Habbena et al. 2009; Horak et al. 2013). Together, these data help to explain accumulations of NO_2^- in the PNM despite active nitrification and provide a mechanistic basis for explaining the observed relationship between f_w and PNM NO_2^-.

Conclusions

The contribution of EZ-based nitrification was estimated from two CCE cruises using concurrent measurements of the $\delta^{15}N$ and $\delta^{18}O$ of nitrate. Results indicated that nitrification contributed between 6% and 36% to the nitrate reservoir between the surface and RML (~ 50–60 m for Cycles < 75 km from shore), with estimated integrated nitrification rates between 0.33 and 2.07 mmol N m^{-2} d^{-1}. These EZ nitrification rates were comparable to those previously reported for the central California Current (e.g., Santoro et al. 2010; Smith et al. 2016).

A simple box model used to examine the possible advection of the isotope signal associated with nitrification into the EZ from source waters indicated that nitrification was likely occurring up to surface depths. Geochemical data primarily required EZ nitrification rates of 2–50 (up to 103) nmol L^{-1} d^{-1}, similar to ammonia and nitrite oxidation rates that have been previously reported for the California Current System (Ward et al. 1982; Santoro et al. 2010; Smith et al. 2014*a*,*b*, 2016). The EZ detection of transcripts related to ammonia oxidation, *amoA*, corresponded with the detection of geochemical-based estimates of complete nitrification for some Cycles, suggesting that active EZ nitrification was occurring in these water masses. Based on our estimates of the contribution of EZ nitrification (recycled nitrogen) to the EZ nitrate pool, new production rates that utilize EZ NO_3^- (e.g., Harrison et al. 1987) could be overestimated by approximately 20%.

Building on an observed positive correlation between geochemical estimates of nitrification and NO_2^- at the PNM, the longer term CalCOFI NO_2^- record was used to infer the temporal evolution of mean nitrification in the southern CCS and CCE regions. Furthermore, a correlation approach was used to identify potential biogeochemical drivers of PNM NO_2^- in the CalCOFI region. This analysis showed that often, PNM NO_2^- accumulation was positively correlated with PON and/or POC:Chl *a*. In the first case, excess PON may serve as an important substrate for ammonia oxidation when ammonium is released during heterotrophic activity. In the second case, reduced Chl *a* (i.e., elevated POC:Chl *a*) could indicate reduced competition with phytoplankton for NH_4^+ and/or NO_2^-. Overall, these processes led to higher nitrite accumulation, which could drive increased nitrite oxidation/nitrification in the EZ.

The analysis presented here based on the natural abundance of $\delta^{15}N$ and $\delta^{18}O$ of nitrate has provided evidence that nitrification within the EZ of the CCE commonly contributes to the EZ NO_3^- reservoir. To further verify the patterns observed here, we recommend that future studies that employ natural abundance stable isotopes of nitrate also concurrently measure gene abundance and expression, and ammonia and nitrite oxidation rates. In addition, identifying the role of PON and NO_2^- uptake by phytoplankton in controlling NO_2^- accumulation, and by extension nitrification, should be a priority to better parameterize the role of nitrification in models of nitrogen cycling in these climatically sensitive environments.

Data availability statement

Data used in this manuscript can be found on the CCE LTER Datazoo website (http://cce.lternet.edu/data) and on the CalCOFI website (calcofi.org).

References

Altabet, M. A. 2001. Nitrogen isotopic evidence for micronutrient control of fractional NO_3^- utilization in the equatorial Pacific. Limnol. Oceanogr. **46**: 368–380. doi:10.4319/lo.2001.46.2.0368

Altabet, M. A., C. Pilskaln, R. Thunell, C. Pride, D. Sigman, F. Chavez, and R. Francois. 1999. The nitrogen isotope biogeochemistry of sinking particles from the margin of the eastern North Pacific. Deep-Sea Res. Part I Oceanogr. Res. Pap. **46**: 655–679. doi:10.1016/S0967-0637(98)00084-3

Beman, J. M., B. N. Popp, and C. A. Francis. 2008. Molecular and biogeochemical evidence for ammonia oxidation by marine Crenarchaeota in the Gulf of California. ISME J. **2**: 429–441. doi:10.1038/ismej.2007.118

Beman, J. M., B. N. Popp, and S. E. Alford. 2012. Quantification of ammonia oxidation rates and ammonia-oxidizing archaea and bacteria at high resolution in the Gulf of California and eastern tropical North Pacific Ocean. Limnol. Oceanogr. **57**: 711–726. doi:10.4319/lo.2012.57.3.0711

Beman, J. M., J. Leilei Shih, and B. N. Popp. 2013. Nitrite oxidation in the upper water column and oxygen minimum

zone of the eastern tropical North Pacific Ocean. ISME J. **7**: 2192–2205. doi:10.1038/ismej.2013.96

Bond, N. A., M. F. Cronin, H. Freeland, and N. Mantua. 2015. Causes and impacts of the 2014 warm anomaly in the NE Pacific. Geophys. Res. Lett. **42**: 3414–3420. doi:10.1002/2015GL063306

Buchwald, C., and K. L. Casciotti. 2010. Oxygen isotopic fractionation and exchange during bacterial nitrite oxidation. Limnol. Oceanogr. **55**: 1064–1074. doi:10.4319/lo.2010.55.3.1064

Buchwald, C., A. E. Santoro, M. R. McIlvin, and K. L. Casciotti. 2012. Oxygen isotopic composition of nitrate and nitrite produced by nitrifying cocultures and natural marine assemblages. Limnol. Oceanogr. **57**: 1361–1375. doi:10.4319/lo.2012.57.5.1361

Casciotti, K. L. 2009. Inverse kinetic isotope fractionation during bacterial nitrite oxidation. Geochim. Cosmochim. Acta **73**: 2061–2076. doi:10.1016/j.gca.2008.12.022

Casciotti, K. L. 2016. Nitrogen and oxygen isotopic studies of the marine nitrogen cycle. Ann. Rev. Mar. Sci. **8**: 379–407. doi:10.1146/annurev-marine-010213-135052

Casciotti, K. L., D. M. Sigman, M. G. Hastings, J. K. Böhlke, and A. Hilkert. 2002. Measurement of the oxygen isotopic composition of nitrate in seawater and freshwater using the denitrifier method. Anal. Chem. **74**: 4905–4912. doi:10.1021/ac020113w

Chavez, F. P., R. T. Barber, and M. P. Sanderson. 1989. The potential primary production of the Peruvian upwelling ecosystem, 1953-1984. Peruvian Upwelling Ecosyst. Dyn. Interact. **18**: 50–63.

Church, M. J., B. Wai, D. M. Karl, and E. F. DeLong. 2010. Abundances of crenarchaeal *amoA* genes and transcripts in the Pacific Ocean. Environ. Microbiol. **12**: 679–688. doi:10.1111/j.1462-2920.2009.02108.x

Cole, S. T., D. L. Rudnick, and J. A. Colosi. 2010. Seasonal evolution of upper-ocean horizontal structure and the remnant mixed layer. J. Geophys. Res. Oceans **115**: 1–15. doi:10.1029/2009JC005654

Collins, L. E., W. Berelson, D. E. Hammond, A. Knapp, R. Schwartz, and D. Capone. 2011. Particle fluxes in San Pedro Basin, California: A four-year record of sedimentation and physical forcing. Deep-Sea Res. Part I Oceanogr. Res. Pap. **58**: 898–914. doi:10.1016/j.dsr.2011.06.008

Daims, H., and others. 2015. Complete nitrification by *Nitrospira* bacteria. Nature **528**: 504–509. doi:10.1038/nature16461

Daims, H., S. Lücker, and M. Wagner. 2016. A new perspective on microbes formerly known as nitrite-oxidizing bacteria. Trends Microbiol. **24**: 699–712. doi:10.1016/j.tim.2016.05.004

Dore, J. E., and D. M. Karl. 1996. Nitrification in the euphotic zone as a source for nitrite, nitrate, and nitrous oxide at Station ALOHA. Limnol. Oceanogr. **41**: 1619–1628. doi:10.4319/lo.1996.41.8.1619

Dugdale, R. C., and J. J. Goering. 1967. Uptake of new and regenerated forms of nitrogen in primary productivity. Limnol. Oceanogr. **12**: 196–206. doi:10.4319/lo.1967.12.2.0196

Eppley, R. W., and B. J. Peterson. 1979. Particulate organic matter flux and planktonic new production in the deep ocean. Nature **282**: 677–680. doi:10.1038/282677a0

Fawcett, S. E., B. B. Ward, M. W. Lomas, and D. M. Sigman. 2015. Vertical decoupling of nitrate assimilation and nitrification in the Sargasso Sea. Deep-Sea Res. Part I Oceanogr. Res. Pap. **103**: 64–72. doi:10.1016/j.dsr.2015.05.004

Francis, C. A., J. M. Beman, and M. M. M. Kuypers. 2007. New processes and players in the nitrogen cycle: The microbial ecology of anaerobic and archaeal ammonia oxidation. ISME J. **1**: 19–27. doi:10.1038/ismej.2007.8

Fripiat, F., and others. 2015. Significant mixed layer nitrification in a natural iron-fertilized bloom of the Southern Ocean. Global Biogeochem. Cycles **29**: 1929–1943. doi:10.1002/2014GB005051

Goericke, R. 2002. Top-down control of phytoplankton biomass and community structure in the monsoonal Arabian Sea. Limnol. Oceanogr. **47**: 1307–1323. doi:10.4319/lo.2002.47.5.1307

Goericke, R., and M. D. Ohman. 2015. Introduction to CCE-LTER: Responses of the California Current Ecosystem to climate forcing. Deep-Sea Res. Part II Top. Stud. Oceanogr. **112**: 1–5. doi:10.1016/j.dsr2.2014.12.001

Granger, J., D. M. Sigman, J. A. Needoba, and P. J. Harrison. 2004. Coupled nitrogen and oxygen isotope fractionation of nitrate during assimilation by cultures of marine phytoplankton. Limnol. Oceanogr. **49**: 1763–1773. doi:10.4319/lo.2004.49.5.1763

Granger, J., D. M. Sigman, M. G. Prokopenko, M. F. Lehmann, and P. D. Tortell. 2006. A method for nitrite removal in nitrate N and O isotope analyses. Limnol. Oceanogr.: Methods **4**: 205–212. doi:10.4319/lom.2006.4.205

Granger, J., D. M. Sigman, M. M. Rohde, M. T. Maldonado, and P. D. Tortell. 2010. N and O isotope effects during nitrate assimilation by unicellular prokaryotic and eukaryotic plankton cultures. Geochim. Cosmochim. Acta **74**: 1030–1040. doi:10.1016/j.gca.2009.10.044

Granger, J., and S. D. Wankel. 2016. Isotopic overprinting of nitrification on denitrification as a ubiquitous and unifying feature of environmental nitrogen cycling. Proc. Natl. Acad. Sci. USA **113**: E6391–E6400. doi:10.1073/PNAS.1601383113

Harrison, W. G., T. Platt, and M. R. Lewis. 1987. f-ratio and its relation to ambient nitrate concentration in coastal waters. J. Plankton Res. **9**: 235–248. doi:10.1093/plankt/9.1.235

Haskell, W. Z., M. G. Prokopenko, D. E. Hammond, R. H. R. Stanley, W. M. Berelson, J. J. Baronas, J. C. Fleming, and L. I. Aluwihare. 2016. An organic carbon budget for coastal Southern California determined by estimates of vertical nutrient flux, net community production and export.

Deep-Sea Res. Part I Oceanogr. Res. Pap. **116**: 49–76. doi:10.1016/j.dsr.2016.07.003

Horak, R. E. A., W. Qin, A. J. Schauer, E. V. Armbrust, A. E. Ingalls, J. W. Moffett, D. A. Stahl, and A. H. Devol. 2013. Ammonia oxidation kinetics and temperature sensitivity of a natural marine community dominated by Archaea. ISME J. **7**: 2023–2033. doi:10.1038/ismej.2013.75

Jacox, M. G., E. L. Hazen, K. D. Zaba, D. L. Rudnick, C. A. Edwards, A. M. Moore, and S. J. Bograd. 2016. Impacts of the 2015–2016 El Niño on the California Current System: Early assessment and comparison to past events. Geophys. Res. Lett. **43**: 7072–7080. doi:10.1002/2016GL069716

Kahru, M., R. Kudela, M. Manzano-Sarabia, and B. G. Mitchell. 2009. Trends in primary production in the California Current detected with satellite data. J. Geophys. Res. Oceans **114**: 1–7. doi:10.1029/2008JC004979

Könneke, M., A. E. Bernhard, J. R. De La Torre, C. B. Walker, J. B. Waterbury, and D. A. Stahl. 2005. Isolation of an autotrophic ammonia-oxidizing marine archaeon. Nature **437**: 543–546. doi:10.1038/nature03911

Landry, M. R., M. D. Ohman, R. Goericke, M. R. Stukel, and K. Tsyrklevich. 2009. Lagrangian studies of phytoplankton growth and grazing relationships in a coastal upwelling ecosystem off Southern California. Prog. Oceanogr. **83**: 208–216. doi:10.1016/j.pocean.2009.07.026

Lomas, M. W., and F. Lipschultz. 2006. Forming the primary nitrite maximum: Nitrifiers or phytoplankton? Limnol. Oceanogr. **51**: 2453–2467. doi:10.4319/lo.2006.51.5.2453

Lücker, S., B. Nowka, T. Rattei, E. Spieck, and H. Daims. 2013. The genome of *Nitrospina gracilis* illuminates the metabolism and evolution of the major marine nitrite oxidizer. Front. Microbiol. **4**: 1–19. doi:10.3389/fmicb.2013.00027

Martens-Habbena, W., P. M. Berube, H. Urakawa, J. R. De La Torre, and D. A. Stahl. 2009. Ammonia oxidation kinetics determine niche separation of nitrifying Archaea and Bacteria. Nature **461**: 976–979. doi:10.1038/nature08465

Messié, M., J. Ledesma, D. D. Kolber, R. P. Michisaki, D. G. Foley, and F. P. Chavez. 2009. Potential new production estimates in four eastern boundary upwelling ecosystems. Prog. Oceanogr. **83**: 151–158. doi:10.1016/j.pocean.2009.07.018

Messié, M., and F. P. Chavez. 2015. Seasonal regulation of primary production in eastern boundary upwelling systems. Prog. Oceanogr. **134**: 1–18. doi:10.1016/j.pocean.2014.10.011

Mincer, T. J., M. J. Church, L. T. Taylor, C. Preston, D. M. Karl, and E. F. DeLong. 2007. Quantitative distribution of presumptive archaeal and bacterial nitrifiers in Monterey Bay and the North Pacific Subtropical Gyre. Environ. Microbiol. **9**: 1162–1175. doi:10.1111/j.1462-2920.2007.01239.x

Montoya, J. P., S. G. Korrigan, and J. J. McCarthy. 1991. Rapid, storm-induced changes in the natural abundance of ^{15}N in a planktonic ecosystem, Chesapeake Bay, USA. Geochim. Cosmochim. Acta **55**: 3627–3638. doi:10.1016/0016-7037(91)90060-I

Nevison, C. D., T. J. Lueker, and R. F. Weiss. 2004. Quantifying the nitrous oxide source from coastal upwelling. Global Biogeochem. Cycles **18**: 1–17. doi:10.1029/2003GB002110

Peng, X., S. E. Fawcett, N. van Oostende, M. J. Wolf, D. Marconi, D. M. Sigman, and B. B. Ward. 2018. Nitrogen uptake and nitrification in the subarctic North Atlantic Ocean. Limnol. Oceanogr. **63**: 1462–1487. doi:10.1002/lno.10784

Pennington, J. T., G. E. Friederich, C. G. Castro, C. A. Collins, W. W. Evans, and F. P. Chavez. 2010. The northern and central California coastal upwelling system, p. 29–44. *In* K. K. Liu, L. Atkinson, R. Quinones, and L. Talaue-McManus [eds.], Carbon and nutrient fluxes in continental margins. Springer Science & Business Media.

Plattner, G.-K., N. Gruber, H. Frenzel, and J. C. McWilliams. 2005. Decoupling marine export production from new production. Geophys. Res. Lett. **32**: L11612. doi:10.1029/2005GL022660

Rafter, P. A., and D. M. Sigman. 2016. Spatial distribution and temporal variation of nitrate nitrogen and oxygen isotopes in the upper equatorial Pacific Ocean. Limnol. Oceanogr. **61**: 14–31. doi:10.1002/lno.10152

Santoro, A. E., K. L. Casciotti, and C. A. Francis. 2010. Activity, abundance and diversity of nitrifying archaea and bacteria in the central California Current. Environ. Microbiol. **12**: 1989–2006. doi:10.1111/j.1462-2920.2010.02205.x

Santoro, A. E., and K. L. Casciotti. 2011. Enrichment and characterization of ammonia-oxidizing archaea from the open ocean: Phylogeny, physiology and stable isotope fractionation. ISME J. **5**: 1796–1808. doi:10.1038/ismej.2011.58

Santoro, A. E., and others. 2013. Measurements of nitrite production in and around the primary nitrite maximum in the central California Current. Biogeosciences **10**: 7395–7410. doi:10.5194/bg-10-7395-2013

Santoro, A. E., R. A. Richter, and C. L. Dupont. 2018. Planktonic marine archaea. Ann. Rev. Mar. Sci. **11**: 131–158. doi:10.1146/annurev-marine-121916-063141

Schleper, C., G. Jurgens, and M. Jonuscheit. 2005. Genomic studies of uncultivated archaea. Nat. Rev. Microbiol. **3**: 479–488. doi:10.1038/nrmicro1159

Sigman, D. M., M. A. Altabet, D. C. McCorkle, R. Francois, and G. Fischer. 1999. The $\delta^{15}N$ of nitrate in the Southern Ocean: Consumption of nitrate in surface waters. Global Biogeochem. Cycles **13**: 1149–1166. doi:10.1029/1999GB900038

Sigman, D. M., K. L. Casciotti, M. Andreani, C. Barford, M. Galanter, and J. K. Böhlke. 2001. A bacterial method for the nitrogen isotopic analysis of nitrate in seawater and freshwater. Anal. Chem. **73**: 4145–4153. doi:10.1021/ac010088e

Sigman, D. M., J. Granger, P. J. DiFiore, M. M. Lehmann, R. Ho, G. Cane, and A. van Geen. 2005. Coupled nitrogen and oxygen isotope measurements of nitrate along the

eastern North Pacific margin. Global Biogeochem. Cycles **19**: 1–14. doi:10.1029/2005GB002458

Sigman, D. M., K. L. Karsh, and K. L. Casciotti. 2010. Nitrogen isotopes in the ocean, p. 40–54. *In* J. H. Steele, K. K. Turekian, and S. A. Thorpe [eds.], Encyclopedia of ocean sciences. 2nd ed. Academic Press. doi:10.1016/B978-012374473-9.00632-9.

Smart, S. M., S. E. Fawcett, S. J. Thomalla, M. A. Weigand, C. J. C. Reason, and D. M. Sigman. 2015. Isotopic evidence for nitrification in the Antarctic winter mixed layer. Global Biogeochem. Cycles **29**: 427–445. doi:10.1002/2014GB005013

Smith, J. M., K. L. Casciotti, F. P. Chavez, and C. A. Francis. 2014*a*. Differential contributions of archaeal ammonia oxidizer ecotypes to nitrification in coastal surface waters. ISME J. **8**: 1704–1714. doi:10.1038/ismej.2014.11

Smith, J. M., F. P. Chavez, and C. A. Francis. 2014*b*. Ammonium uptake by phytoplankton regulates nitrification in the sunlit ocean. PLoS One **9**: 1–9. doi:10.1371/journal.pone.0108173

Smith, J. M., J. Damashek, F. P. Chavez, and C. A. Francis. 2016. Factors influencing nitrification rates and the abundance and transcriptional activity of ammonia-oxidizing microorganisms in the dark northeast Pacific Ocean. Limnol. Oceanogr. **61**: 596–609. doi:10.1002/lno.10235

Stephens, B. M., M. Porrachia, S. Dovel, M. Roadman, R. Goericke, and L. I. Aluwihare. 2018. Nonsinking organic matter production in the California Current. Global Biogeochem. Cycles **32**: 1386–1405. doi:10.1029/2018GB005930

Stukel, M. R., M. R. Landry, C. R. Benitez-Nelson, and R. Goericke. 2011. Trophic cycling and carbon export relationships in the California Current Ecosystem. Limnol. Oceanogr. **56**: 1866–1878. doi:10.4319/lo.2011.56.5.1866

Stukel, M. R., and others. 2017. Mesoscale ocean fronts enhance carbon export due to gravitational sinking and subduction. Proc. Natl. Acad. Sci. USA **114**: 1252–1257. doi:10.1073/pnas.1609435114

Stukel, M. R., H. Song, R. Goericke, and A. J. Miller. 2018. The role of subduction and gravitational sinking in particle export, carbon sequestration, and the remineralization length scale in the California Current Ecosystem. Limnol. Oceanogr. **63**: 363–383. doi:10.1002/lno.10636

Sugimoto, R., A. Kasai, T. Miyajima, and K. Fujita. 2009. Controlling factors of seasonal variation in the nitrogen isotope ratio of nitrate in a eutrophic coastal environment. Estuar. Coast. Shelf Sci. **85**: 231–240. doi:10.1016/j.ecss.2009.08.006

Sun, X., Q. Ji, A. Jayakumar, and B. B. Ward. 2017. Dependence of nitrite oxidation on nitrite and oxygen in low-oxygen seawater. Geophys. Res. Lett. **44**: 7883–7891. doi:10.1002/2017GL074355

Todd, R. E., D. L. Rudnick, M. R. Mazloff, B. D. Cornuelle, and R. E. Davis. 2012. Thermohaline structure in the California Current System: Observations and modeling of spice variance. J. Geophys. Res. Oceans **117**: C02008. doi:10.1029/2011JC007589

Vokhshoori, N. L., and M. D. McCarthy. 2014. Compound-specific δ^{15}N amino acid measurements in littoral mussels in the California upwelling ecosystem: A new approach to generating baseline δ^{15}N isoscapes for coastal ecosystems. PLoS One **9**: e98087. doi:10.1371/journal.pone.0098087

Wankel, S. D., C. Kendall, J. T. Pennington, F. P. Chavez, and A. Paytan. 2007. Nitrification in the euphotic zone as evidenced by nitrate dual isotopic composition: Observations from Monterey Bay, California. Global Biogeochem. Cycles **21**: 1–13. doi:10.1029/2006GB002723

Ward, B. B. 1985. Light and substrate concentration relationships with marine ammonium assimilation and oxidation rates. Mar. Chem. **16**: 301–316. doi:10.1016/0304-4203(85)90052-0

Ward, B. B. 1987. Nitrogen transformations in the Southern California Bight. Deep-Sea Res. A **34**: 785–805. doi:10.1016/0198-0149(87)90037-9

Ward, B. B. 2005. Temporal variability in nitrification rates and related biogeochemical factors in Monterey Bay, California, USA. Mar. Ecol. Prog. Ser. **292**: 97–109. doi:10.3354/meps292097

Ward, B. B. 2008. Nitrification in marine systems, p. 199–261. *In* D.G. Capone, D.A. Bronk, M.R. Mulholland, and E.J. Carpenter [eds.], Nitrogen in the Marine Environment. Academic Press. doi:10.1016/B978-0-12-372522-6.00005-0.

Ward, B. B., R. J. Olson, and M. J. Perry. 1982. Microbial nitrification rates in the primary nitrite maximum off southern California. Deep-Sea Res. A **29**: 247–255. doi:10.1016/0198-0149(82)90112-1

Ward, B. B., M. C. Talbot, and M. J. Perry. 1984. Contributions of phytoplankton and nitrifying bacteria to ammonium and nitrite dynamics in coastal waters. Cont. Shelf Res. **3**: 383–398. doi:10.1016/0278-4343(84)90018-9

Ward, B. B., and A. F. Carlucci. 1985. Marine ammonia- and nitrite-oxidizing bacteria: Serological diversity determined by immunofluorescence in culture and in the environment. Appl. Environ. Microbiol. **50**: 194–201.

Ward, B. B., K. A. Kilpatrick, E. H. Renger, and R. W. Eppley. 1989. Biological nitrogen cycling in the nitracline. Limnol. Oceanogr. **34**: 493–513. doi:10.4319/lo.1989.34.3.0493

Watson, S. W., and J. B. Waterbury. 1971. Characteristics of two marine nitrite oxidizing bacteria, *Nitrospina gracilis nov. gen. nov. sp.* and *Nitrococcus mobilis nov. gen. nov. sp.* Arch. Mikrobiol. **77**: 203–230. doi:10.1007/BF00408114

Willis, J. K., and others. 2007. Climate change 2007: The physical science basis. Contribution of working group I to the fourth assessment report of the Intergovernmental Panel on Climate Change. Cambridge Univ. Press.

Xia, F., J.-G. Wang, T. Zhu, B. Zou, S.-K. Rhee, and Z.-X. Quan. 2018. Ubiquity and diversity of complete ammonia oxidizers (comammox). Appl. Environ. Microbiol. **84**: e01390–e01318. doi:10.1128/aem.01390-18

Yool, A., A. P. Martin, C. Fernández, and D. R. Clark. 2007. The significance of nitrification for oceanic new production. Nature **447**: 999–1002. doi:10.1038/nature05885

Zaba, K. D., and D. L. Rudnick. 2016. The 2014-2015 warming anomaly in the Southern California Current System observed by underwater gliders. Geophys. Res. Lett. **43**: 1241–1248. doi:10.1002/2015GL067550

Zakem, E. J., and others. 2018. Ecological control of nitrite in the upper ocean. Nat. Commun. **9**: 1206–1213. doi:10.1038/s41467-018-03553-w

Acknowledgments

We gratefully thank colleagues in the CalCOFI and CCE LTER programs who contributed substantially to our seagoing program, analyses conducted in the laboratory, and for making the long-term inorganic nutrient context possible. We especially acknowledge Sara Rivera who provided significant support for samples collected during the 2016 field campaign, and Bruce Deck, Megan Roadman, and Shonna Dovel for the collection and analysis of POM samples for the CalCOFI Program. We would also like to thank Alyson Santoro and Carly Buchwald for their thoughtful comments on the primary discussion points presented here. We also thank the captains and crews of the R/V *Melville*, R/V *Revelle*, and R/V *Sikuliaq*. Finally, we must acknowledge the substantial feedback from an *L&O* editor and two anonymous reviewers that significantly improved the readability and presentation of this manuscript. This work was funded by NSF Biological Oceanography grants to the CCE LTER Program: OCE-0417616, OCE-1637632, and OCE-1614359. Funding for this research was also provided by National Science Foundation (NSF-OCE-1756884), NOAA (NA15OAR4320071) and Gordon and Betty Moore Foundation grants (GBMF3828) to AEA.

Conflict of Interest

None declared.

Submitted 21 December 2018
Revised 08 July 2019
Accepted 14 September 2019

Associate editor: Bo Thamdrup